A kind of NiTi-wire shape memory alloy damper to simultaneously damp tension, compression and torsion

Yu-Lin Han[†], Hai-Yang Yin[‡], Er-Tian Xiao[‡], Zhi-Lin Sun[‡] and Ai-Qun Li[‡†]

College of Civil Engineering, Southeast University, Nanjing City 210096, P. R. China

Abstract. NiTi-wire shape memory alloy (SMA) dampers, that utilize NiTi SMA wires to simultaneously damp tension, compression and torsion, was developed for structural control implementation in this study. First, eight reduced-scale NiTi-wire SMA dampers were constructed. Then tension, compression and torsion experiments using the eight reduced-scale NiTi-wire SMA dampers of different specification were done. The experimental results revealed all of the eight reduced-scale NiTi-wire SMA dampers had the ability to simultaneously supply tension-compression damping and torsion damping. Finally, mechanics analysis of the NiTi-wire SMA dampers was done based on a model of the SMA-wire restoring force and on tension-compression and torsion damping analysis. The damping analytical results were found to be similar to the damping experimental results.

Key words: shape memory alloys (SMA); smart materials; smart structures; damper; structural control; vibration; earthquake.

1. Introduction

SMA has been mainly applied in medical science, and in electrical, aerospace and mechanical engineering. Graesser and Cozzarelli (1991) explored the possibility of using SMA as new materials for seismic isolation. Experimental and theoretical studies have been recently done on exploiting SMA-based devices for structural control implementation; e.g., Aiken *et al.* (1993), Witting and Cozzarelli (1992), Hodgson and Krumme (1994), Dolce *et al.* (2000), Duval *et al.* (2000). Dolce *et al.* (2000) gave a state-of-the-art review of the development of passive control devices based on SMA up to 1999. Only recent works directly related to our study are therefore mentioned here.

Duval *et al.* (2000) studied the dynamic behavior of a single-degree-of-freedom (SDOF) mechanical system, which uses an SMA spring as a restoring force element. Van Humbeeck and Liu (2000) reported that the damping capacity of SMA increases with increasing amplitude of vibration or applied impact and is relatively frequency independent. Adachi *et al.* (2000) developed a damping device made SMA, which can absorb seismic energy and reduce the seismic force by its

pseudo yield effect. Ip (2000) proposed an analytical formula to predict the energy dissipation in Ni-Ti shape memory alloy wires under cyclic bending. Han *et al.* (2000) utilized plastic deformation of SMA to absorb vibration energy of a frame. Saadat *et al.* (2001) used NiTi SMA tendons for vibration control of coastal structures. Ostachowicz and Kaczmarczyk (2001) proposed a finite element model to predict the dynamic response of composite plates with embedded SMA fibres. Tamai and Kitagawa (2002) developed seismic-resistant members that utilize SMAs, such as braces and exposed-type column bases, as hysteretic dampers for building structures. Torra *et al.* (2002) analytically studied damping via Cu-Zn-Al SMAs and confirmed the alloy properties of these SMAs for a series of working cycles separated by long periods in austenite phase for rare evens, such as earthquakes. Han *et al.* (2003) developed a damper based on SMA wires for structural control implementation; Eight of these NiTi-wire SMA dampers were installed in a frame structure to verify the effectiveness of the damper. Williams *et al.* (2005) discussed the development and modeling of a continuously tuned SMA adaptive tuned vibration absorber utilizing an R-phase transformation to realize online variation of the ATVA natural frequency.

In this study, an SMA damper was developed that uses wires made of an SMA alloy, NiTi, to simultaneously damp tension-compression and torsion. Eight reduced-scale NiTi-wire dampers of different specification were constructed. Damping force, damping torque and energy dissipation ability of these dampers in tension-compression and torsion (i.e., displacement, torsion-angle displacement, deformation, restoring force, damping force and damping torque) were measured, and then compared with analytical results based on a model of pseudoelasticity restoring force for an SMA wire and on tension-compression and torsion analysis. Here, firstly, construction of the reduced-scale NiTi-wire SMA dampers is described. Then, the energy dissipation principle of a NiTi-wire SMA damper under tension, compression or torsion is described. Finally, comparison between the analytical and measured results is presented. The analytical results were similar with measured results. The measured and analytical results revealed the following features of the NiTi-wire SMA dampers. All the eight reduced-scale NiTi-wire SMA dampers could simultaneously damp tension-compression and torsion. When the distance d_1 between two SMA NiTi-wires increased (d_1 in Fig. 1), the dissipated vibration energy of NiTi-wire SMA damper decreased. When distance d_1 increased, the maximum damping force F_{max} and the maximum damping torque T_{max} increased sensitively too. The maximum displacement δ_{max} and the maximum angle displacement θ_{max} almost were independent of d_1. The reason for this independence is that the measured and analytical results of all dampers were based on the same condition that the long SMA wire of all the measured NiTi-wire SMA dampers was deformed along the same force-deformation path. The energy dissipation ratio η for the dampers decreased when d_1 increased.

2. Energy dissipation principle of an NiTi-wire SMA damper

NiTi wires were selected as the energy dissipation material in the NiTi-wire SMA dampers developed here. The pseudoelasticity of SMA wires is used to dissipate vibration energy. Han *et al.* (2003) previously discussed in detail the use of SMA damper for vibration control of a frame based on the SMA pseudoelasticity energy dissipation principle.

The NiTi-wire SMA dampers developed here (Figs. 1 and 2) can simultaneously supply tension-compression damping and torsion damping. When the SMA damper (Fig. 1) is in tension-compression and/or torsion, the SMA wires in the damper will be in tension, and then dissipate
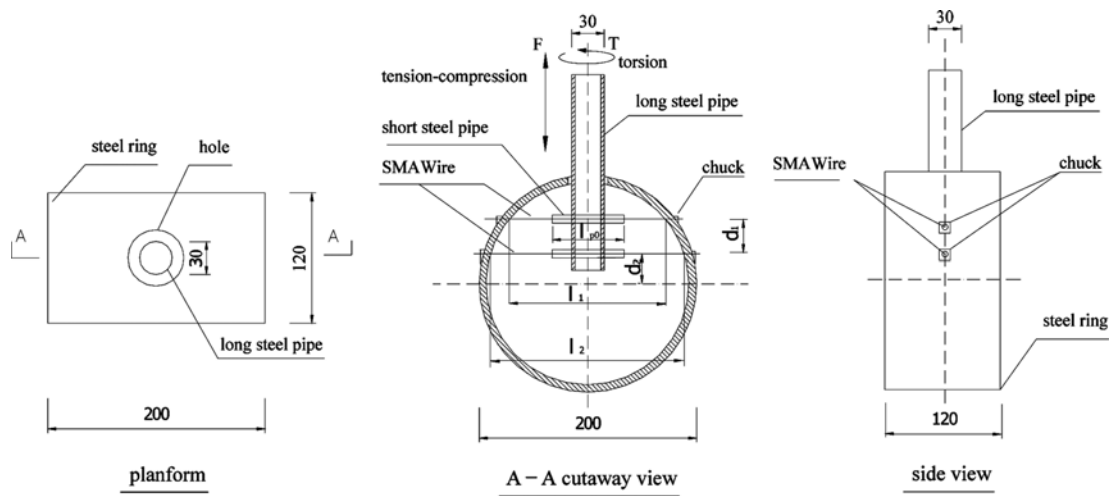
Fig. 1 Reduced-scale NiTi-wire SMA damper (*F*: Force; *T*: Torque)
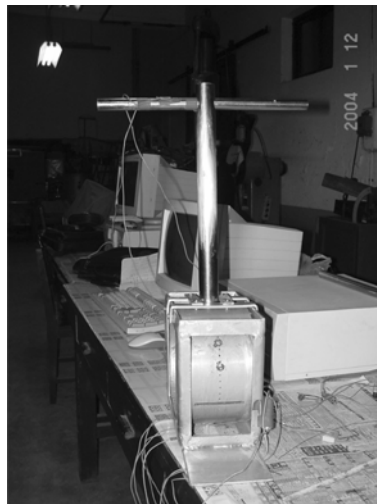

Fig. 2 A Reduced-scale NiTi-wire SMA damper

vibration energy according to the principle previously discussed by Han *et al.* (2003).

The developed NiTi-wire SMA damper can still be in the structures shown by Fig. 3, to supply damping in four directions by four long steel pipes. If the developed NiTi-wire SMA damper is designed as having two or three long pipes, then the damper can supply damping in two or three directions (see sketch in Fig. 4). It is decided by the aim of structure control which kind of NiTi-wire SMA damper (Figs. 1-4) should be selected. For reason of simplification, only the NiTi-wire SMA damper with one long steel pipe (Fig. 1) was discussed in this paper. The dampers, shown in Figs. 3 and 4, can be analyzed by the same method that was used in this paper.
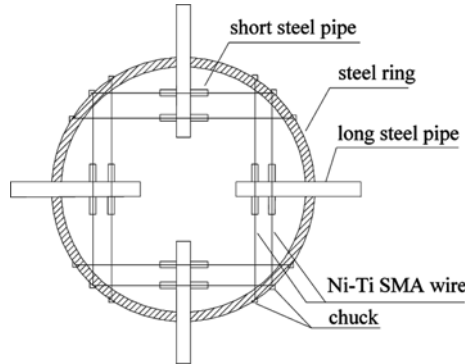
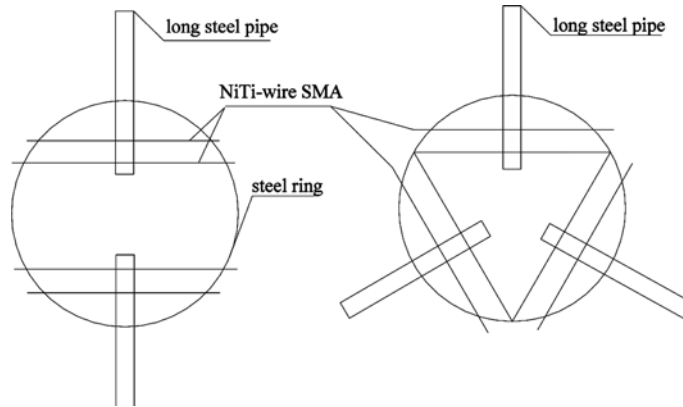Fig. 3 NiTi-wire SMA damper with four long steel pipes

Fig. 4 NiTi-wire SMA damper with two or three long steel pipes (sketch)

3. SMA pseudoelasticity restoring force model

3.1 Pseudoelasticity restoring force curve of NiTi-wire SMA wire

The pseudoelasticity restoring force curve for an NiTi SMA wire (1 mm-diameter, 100 mm-working-length) was determined by measuring the restoring force, f, as a function of deformation, x, using a general mini material test system at 25°C. Fig. 5 shows the measured curve.

3.2 SMA pseudoelasticity restoring force model

To simplify the calculation of damping properties of NiTi-wire dampers, we used a *triangle restoring force* model (Fig. 6) that is simplified from a restoring force experiment curve (Figs. 5 and 6). The following conditions are met in this simplification.
 • Simplified restoring force model (Fig. 6) is triangle, which coincides relatively well to the measured restoring force curve (Figs. 5 and 6).
 • Triangle restoring force model has the same maximum restoring force and corresponding
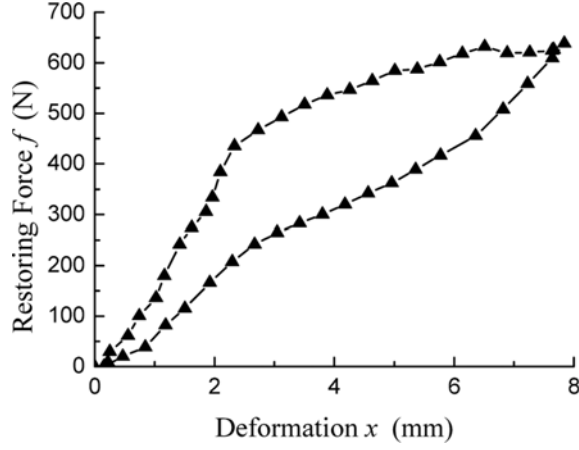
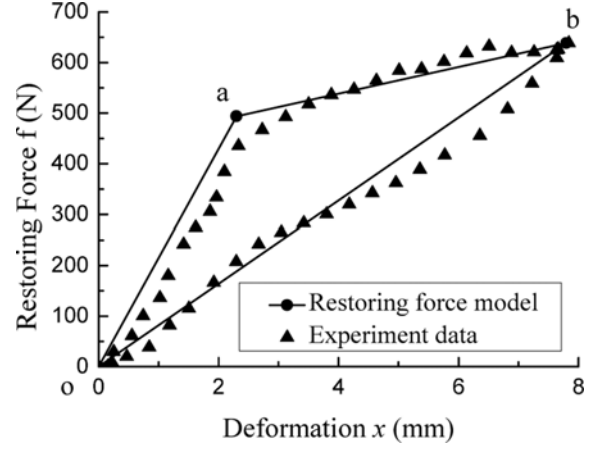Fig. 5 SMA wire pseudoelasticity restoring force curve, 25°C

Fig. 6 Restoring force model

deformation as those of the measured restoring force curve.

• Triangle restoring force model has the same energy dissipation ratio as that of the measured restoring force curve.

The restoring force model (Fig. 6) can be expressed as

$$f(x) = \begin{cases} k_1 x & (oa) \\ (k_1 - k_2)x_a + k_2 x & (ab) \\ k_3 x & (bo) \end{cases} \qquad (1)$$

where $f(x)$ is restoring force, x is deformation of the SMA wire, x_a is the SMA wire deformation at point "a" in Fig. 6, k_1 is the slope of line "oa" in Fig. 6, k_2 is the slope of line "ab" in Fig. 6, and k_3 is the slope of line "bo" in Fig. 6.

The restoring force model, represented in Eq. (1) will be used here to analyze the damping properties (i.e., displacement, angle displacement, deformation, restoring force, damping force, damping torque, damping force moment, and energy dissipation ratio) of the NiTi-wire SMA damper, including the three reduced-scale dampers.

Analysis for the reduced-scale dampers (Fig. 1) is described here. Each damper was constructed from one steel ring, one long steel pipe, one short steel pipe and two crossed 1 mm-diameter 50.2at%NiTi (Ni atom ratio is 50.2%) wires.

A schematic of the reduced-scale damper is shown in Fig. 1. In this paper, F is damping Force, δ is corresponding displacement to damping Force F; T is damping Torque, θ is corresponding angle displacement to damping Torque T; l_1 is the working length of the shorter SMA-wire. l_2 is the working length of the longer SMA-wire (See Figs. 1 and 2 for reference).

According to the restoring force model used here (Fig. 6), $x_a = 2.3$ mm, $f(x_a) = 493.8$ N, $x_b = 7.8$ mm, $f(x_b) = 638.6$ N, $k_1 = 214.7$ N/mm, $k_2 = 26.3$ N/mm, $k_3 = 81.9$ N/mm. For different SMA wire working length (such as l_i mm instead of 100 mm) of SMA wires, the above parameters must be modified to new data (Eq. (2)).

$$\begin{cases} x_{ai} = 2.3l_i/100 \text{ mm} \\ x_{bi} = 7.8l_i/100 \text{ mm} \\ k_{1i} = 214.7 \times 100/l_i \text{ N/mm} \qquad (i = 1, 2) \\ k_{2i} = 26.3 \times 100/l_i \text{ N/mm} \\ k_{3i} = 81.9 \times 100/l_i \text{ N/mm} \end{cases} \qquad (2)$$

To simplify the calculation of damping properties of NiTi-wire SMA damper, only one load cycle of the damper is considered in this analysis. One load cycle is defined as the deformation of the long SMA wire along path *o-a-b-o* (Fig. 6) when the damper is subjected to a damping force or moment.

4. Tension, compression and torsion tests of reduced-scale NiTi-wire SMA dampers

4.1 Reduced-scale SMA dampers

To verify the feasibility of the NiTi-wire SMA damper developed in this paper, eight reduced-scale dampers (Table 1, Figs. 1 and 2) of different specification were constructed. Each damper was constructed from one steel ring, one long steel pipe, one short steel pipe and two crossed 1 mm-diameter 50.2at%NiTi (Ni atom ratio is 50.2%) wires. The specification of the eight reduced-scale dampers is listed in Table 1.
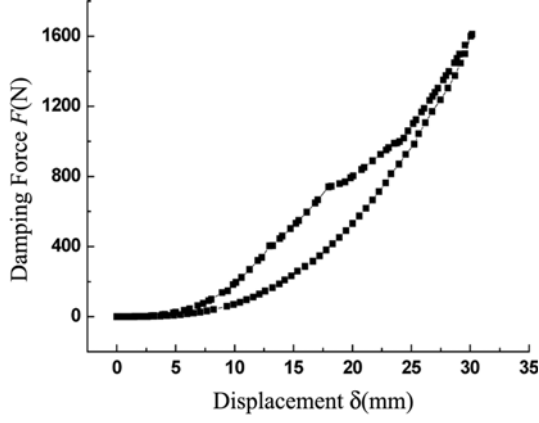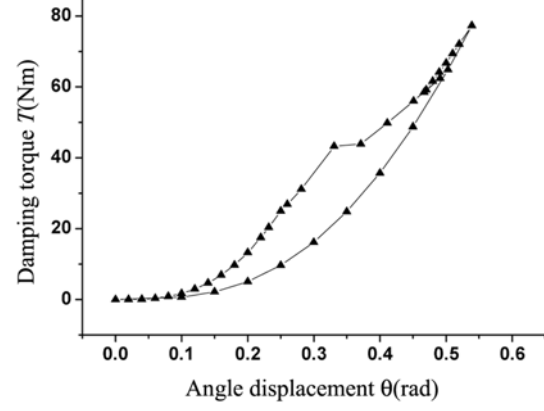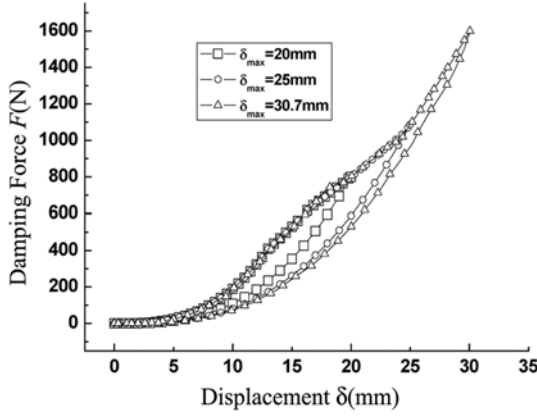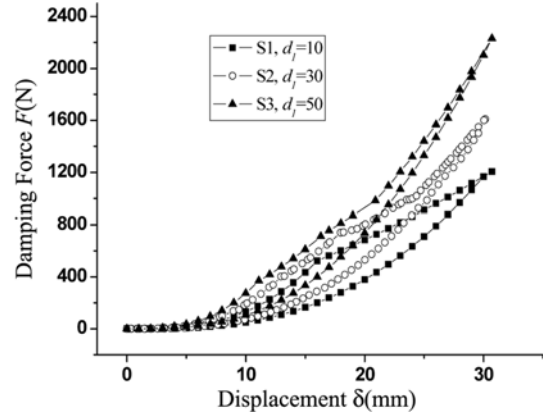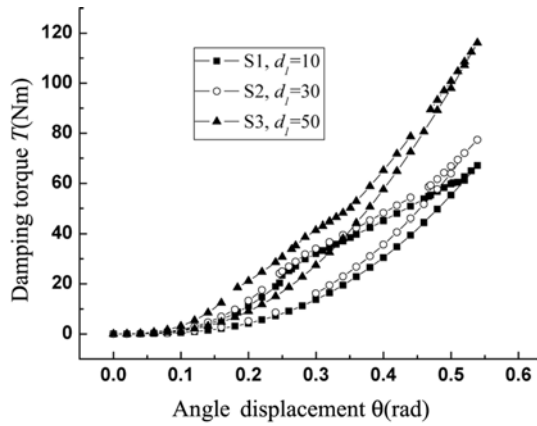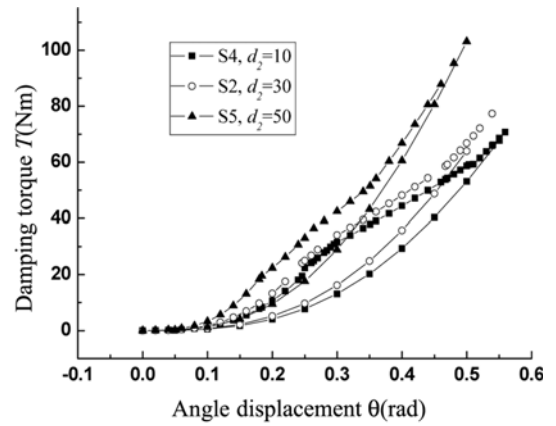
The damping force F, damping torque T, displacement δ, and angle displacement θ of the eight reduced-scale dampers were measured and analyzed in this study.

4.2 Tension, compression and torsion tests of reduced-scale NiTi-wire SMA dampers

Tension, compression and torsion tests were done using the eight reduced-scale NiTi-wire SMA dampers at 25°C (Table 1). A displacement sensor, an angle displacement sensor, a force sensor and a torque sensor were used in the experiment. Measured data was transferred by A/D converter and recorded on a computer. Part of the measured data is illustrated in Figs. 7 to 14 (where F is damping Force, δ is corresponding displacement to damping Force F; T is damping Torque, θ is

Table 1 Eight reduced-scale NiTi-wire SMA dampers

No.	Diameter of steel ring (mm)	Diameter of long steel pipe (mm)	l_{p0} (mm) (Fig. 1)	d_1 (mm) (Fig. 1)	d_2 (mm) (Fig. 1)	Diameter of SMA wire (mm)
S1	200	30	70	10	30	1
S2	200	30	70	30	30	1
S3	200	30	70	50	30	1
S4	200	30	70	30	10	1
S5	200	30	70	30	50	1
S6	200	30	40	30	30	1
S7	200	30	50	30	30	1
S8	200	30	60	30	30	1

Fig. 7 Measured *F~δ* curve of Specimen No. S2

Fig. 8 Measured *T~θ* curve of Specimen No. S2

Fig. 9 Measured *F~δ* curve of Specimen No. S2

Fig. 10 Measured *F~δ* curve of Specimens No. S1, S2 and S3

Fig. 11 Measured *T~θ* curve of Specimens No. S1, S2 and S3

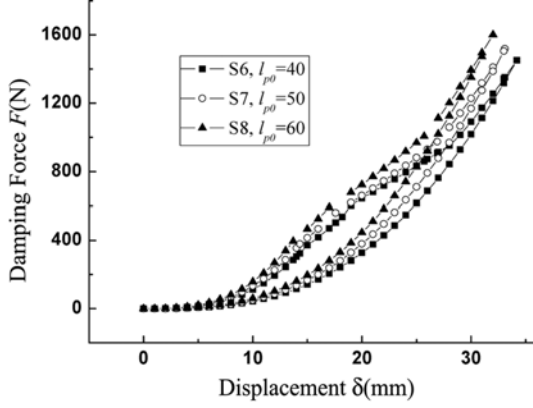Fig. 12 Measured *T~θ* curve of Specimens No. S2, S4 and S5

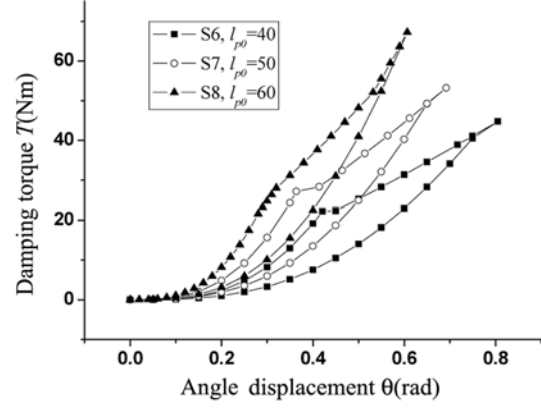Fig. 13 Measured $F\sim\delta$ curve of Specimens No. S6, S7 and S8

Fig. 14 Measured $T\sim\theta$ curve of Specimens No. S6, S7 and S8

corresponding angle displacement to damping Torque T). The other measured data showed similar results, and are therefore not shown. The following conclusions can be got from the measured data.

- All the eight reduced-scale NiTi-wire SMA dampers can supply damping force and damping torque (such as Figs. 7, 8).
- For a given NiTi-wire SMA damper, when the maximum displacement increased, the dissipated vibration energy (illustrated by the area of Force-Displacement Curve in Fig. 9) of damper increased.
- When the distance d_1 between two SMA NiTi-wires increased (d_1 in Fig. 1), the dissipated vibration energy of NiTi-wire SMA damper decreased (Figs. 10, 11).
- When distance d_1 increased, the maximum damping force F_{max} and the maximum damping torque T_{max} increased sensitively (Figs. 8, 9).
- When the parameter d_2 (see Fig. 1) of NiTi-wire SMA damper decreased, the dissipated vibration energy of NiTi-wire SMA damper increased (such as Fig. 12).
- When the parameter l_{p0} (length of short steel pipe, see Fig. 1) of NiTi-wire SMA damper decreased, the energy dissipated ability of NiTi-wire SMA damper increased (such as Figs. 13, 14).
- When l_{p0} and d_2 increased, δ_{max} and θ_{max} decreased, F_{max} and T_{max} increased (such as Figs. 11-14).
- The maximum displacement δ_{max} and the maximum angle displacement θ_{max} almost were independent of d_1 (Figs. 10, 11). The reason for this independence is that the measured results were based on the same condition that the long SMA wire of all the measured NiTi-wire SMA dampers was deformed along the same force-deformation path $o \rightarrow a \rightarrow b \rightarrow o$ (Fig. 6).

5. Mechanics analysis of reduced-scale NiTi-wire SMA dampers

5.1 Tension and compression damping analysis of NiTi-wire SMA damper

5.1.1 Relationship between damping force F and displacement δ of NiTi-wire SMA damper

F is the applied tension-compression force, and δ is the relative displacement between the steel ring and the long steel pipe (Fig. 1). The relationship between deformation x_i of a SMA wire

(original working length l_i) and displacement δ can be expressed as

$$x_i = 2\left(\sqrt{\left(\frac{l_i - l_{p0}}{2}\right)^2 + \delta^2} - \left(\frac{l_i - l_{p0}}{2}\right)\right)$$

then displacement δ can be expressed as

$$\delta = \frac{1}{2}\sqrt{x_i}\sqrt{2l_i + x_i - 2l_{p0}} \tag{3}$$

- When $\delta = \delta_1$, and deformation of short SMA-wire $x_1 = x_{a1} = 2.3l_1/100$ mm, then (See Fig. 6. Using Eqs. (2) and (3))

$$2.3l_1/100 = 2\left(\sqrt{\left(\frac{l_1 - l_{p0}}{2}\right)^2 + \delta_1^2} - \left(\frac{l_1 - l_{p0}}{2}\right)\right)$$

$$\delta_1 = \frac{1}{2}\sqrt{0.023l_1}\sqrt{2l_1 + 0.023l_1 - 2l_{p0}} \tag{4}$$

while deformation of long SMA-wire: $x_2 = 2\left(\sqrt{\left(\frac{l_2 - l_{p0}}{2}\right)^2 + \delta_1^2} - \left(\frac{l_2 - l_{p0}}{2}\right)\right)$

- When $\delta = \delta_2$, and deformation of long SMA-wire $x_2 = x_{a2} = 2.3l_2/100$ mm, then (See Fig. 6 and Eq. (2))

$$\delta_2 = \frac{1}{2}\sqrt{0.023l_2}\sqrt{2l_2 + 0.023l_2 - 2l_{p0}} \tag{5}$$

while deformation of short SMA-wire: $x_1 = 2\left(\sqrt{\left(\frac{l_1 - l_{p0}}{2}\right)^2 + \delta_2^2} - \left(\frac{l_1 - l_{p0}}{2}\right)\right)$

- When $\delta = \delta_3$ and $x_1 = x_{b1} = 7.83l_1/100$ mm, then (See Fig. 6 and Eq. (2))

$$\delta_3 = \frac{1}{2}\sqrt{0.078l_1}\sqrt{2l_1 + 0.078l_1 - 2l_{p0}} \tag{6}$$

while deformation of long SMA-wire: $x_2 = 2\left(\sqrt{\left(\frac{l_2 - l_{p0}}{2}\right)^2 + \delta_3^2} - \left(\frac{l_2 - l_{p0}}{2}\right)\right)$

- When $\delta = \delta_4$, and $x_2 = x_{b2} = 7.83l_1/100$ mm, then (See Fig. 6 and Eq. (2))

$$\delta_4 = \frac{1}{2}\sqrt{0.078l_2}\sqrt{2l_2 + 0.078l_2 - 2l_{p0}} \tag{7}$$

while deformation of short SMA-wire: $x_1 = 2\left(\sqrt{\left(\frac{l_1 - l_{p0}}{2}\right)^2 + \delta_4^2} - \left(\frac{l_1 - l_{p0}}{2}\right)\right)$

The load history of NiTi-wire SMA damper can be divided into the following parts.

a. For $0 \leq \delta \leq \delta_1$
For short SMA-wire ($x_1 \leq x_{a1}$, '*oa*' part of restoring force model of Fig. 6)

$$f_1 = k_{11}x_1 = 2k_{11}\left(\sqrt{\left(\frac{l_1 - l_{p0}}{2}\right)^2 + \delta^2} - \left(\frac{l_1 - l_{p0}}{2}\right)\right)$$

$$F_1 = 2f_{11} * \delta / \sqrt{\left(\frac{l_1 - l_{p0}}{2}\right)^2 + \delta^2}$$

where f_1 is restoring force of short SMA-wire, and F_1 is force applied on long steel pipe (Fig. 1) by short SMA-wire.

For long SMA-wire ($x_2 \leq x_{a2}$, 'oa' part of restoring force model of Fig. 6)

$$f_2 = k_{12}x_2 = 2k_{12}\left(\sqrt{\left(\frac{l_2 - l_{p0}}{2}\right)^2 + \delta^2} - \left(\frac{l_2 - l_{p0}}{2}\right)\right)$$

$$F_2 = 2f_{12} * \delta / \sqrt{\left(\frac{l_2 - l_{p0}}{2}\right)^2 + \delta^2}$$

where f_2 is restoring force of long SMA-wire, and F_2 is force applied on long steel pipe (Fig. 1) by long SMA-wire.

In this part of load history of NiTi-wire SMA damper, the relationship of damping force F and displacement δ of NiTi-wire SMA damper can be expressed by

$$F = F_1 + F_2, \quad \text{then}$$

$$\begin{cases} F = 2f_1 * \delta / \sqrt{\left(\frac{l_1 - l_0}{2}\right)^2 + \delta^2} + 2f_2 * \delta / \sqrt{\left(\frac{l_2 - l_0}{2}\right)^2 + \delta^2} \\ f_1 = 2k_{11}\left(\sqrt{\left(\frac{l_1 - l_0}{2}\right)^2 + \delta^2} - \left(\frac{l_1 - l_0}{2}\right)\right) \qquad (0 < \delta \leq \delta_1) \\ f_2 = 2k_{12}\left(\sqrt{\left(\frac{l_2 - l_0}{2}\right)^2 + \delta^2} - \left(\frac{l_2 - l_0}{2}\right)\right) \end{cases} \quad (8)$$

b. For $\delta_1 \leq \delta \leq \delta_2$
For long SMA-wire ($x_2 \leq x_a$, 'oa' part of restoring force model of Fig. 6)

$$f_2 = k_{12}x_2 = 2k_{12}\left(\sqrt{\left(\frac{l_2 - l_{p0}}{2}\right)^2 + \delta^2} - \left(\frac{l_2 - l_{p0}}{2}\right)\right)$$

$$F_2 = 2f_2 * \delta / \sqrt{\left(\frac{l_2 - l_{p0}}{2}\right)^2 + \delta^2}$$

For short SMA-wire ($x_{a1} \leq x_1 \leq x_{b1}$, 'ab' part of restoring force model of Fig. 6)

$$f_1 = (k_{11} - k_{21})x_a + 2k_{21}\left(\sqrt{\left(\frac{l_1 - l_{p0}}{2}\right)^2 + \delta^2} - \left(\frac{l_1 - l_{p0}}{2}\right)\right)$$

$$F_1 = 2f_1*\delta / \sqrt{\left(\frac{l_1 - l_{p0}}{2}\right)^2 + \delta^2}$$

In this part of load history of NiTi-wire SMA damper, the relationship of damping force F and displacement δ of NiTi-wire SMA damper can be expressed by

$$\begin{cases} F = 2f_1*\delta / \sqrt{\left(\frac{l_1 - l_0}{2}\right)^2 + \delta^2} + 2f_2*\delta / \sqrt{\left(\frac{l_2 - l_0}{2}\right)^2 + \delta^2} \\[2ex] f_1 = (k_{11} - k_{21})x_a + 2k_{21}\left(\sqrt{\left(\frac{l_1 - l_0}{2}\right)^2 + \delta^2} - \left(\frac{l_1 - l_0}{2}\right)\right) \qquad (\delta_1 < \delta \le \delta_2) \\[2ex] f_2 = 2k_{12}\left(\sqrt{\left(\frac{l_2 - l_0}{2}\right)^2 + \delta^2} - \left(\frac{l_2 - l_0}{2}\right)\right) \end{cases} \qquad (9)$$

c. For $\delta_2 \le \delta \le \delta_3$

For short SMA-wire ($x_{a1} \le x_1 \le x_{b1}$, '$ab$' part of restoring force model of Fig. 6)

$$f_1 = (k_{11} - k_{21})x_{a1} + 2k_{21}\left(\sqrt{\left(\frac{l_1 - l_{p0}}{2}\right)^2 + \delta^2} - \left(\frac{l_1 - l_{p0}}{2}\right)\right)$$

$$F_1 = 2f_1*\delta / \sqrt{\left(\frac{l_1 - l_{p0}}{2}\right)^2 + \delta^2}$$

For long SMA-wire ($x_{a2} \le x_2 \le x_{b2}$, '$ab$' part of restoring force model of Fig. 6)

$$f_2 = (k_{12} - k_{22})x_{a2} + 2k_{22}\left(\sqrt{\left(\frac{l_2 - l_{p0}}{2}\right)^2 + \delta^2} - \left(\frac{l_2 - l_{p0}}{2}\right)\right)$$

$$F_2 = 2f_2*\delta / \sqrt{\left(\frac{l_2 - l_{p0}}{2}\right)^2 + \delta^2}$$

In this part of load history of NiTi-wire SMA damper, the relationship of damping force F and displacement δ of NiTi-wire SMA damper can be expressed by

$$\begin{cases} F = 2f_1*\delta / \sqrt{\left(\frac{l_1 - l_0}{2}\right)^2 + \delta^2} + 2f_2*\delta / \sqrt{\left(\frac{l_2 - l_0}{2}\right)^2 + \delta^2} \\[2ex] f_1 = (k_{11} - k_{21})x_{a1} + 2k_{21}\left(\sqrt{\left(\frac{l_1 - l_0}{2}\right)^2 + \delta^2} - \left(\frac{l_1 - l_0}{2}\right)\right) \qquad (\delta_2 < \delta \le \delta_3) \\[2ex] f_2 = (k_{12} - k_{22})x_{a2} + 2k_{22}\left(\sqrt{\left(\frac{l_2 - l_0}{2}\right)^2 + \delta^2} - \left(\frac{l_2 - l_0}{2}\right)\right) \end{cases} \qquad (10)$$

d. For $\delta_3 \le \delta \le \delta_4$. The relationship between restoring force f_1 and deformation x_1 of short wire is linear elasticity. The slope of f-x line of short SMA wire is simplified as k_3, while deformation of long wire is x_2 ($x_{a2} \le x_2 \le x_{b2}$, '$ab$' part of restoring force model of Fig. 6).

For short SMA-wire:

$$f_1 \;=\; k_{31}x_1 \;=\; 2k_{31}\Big(\sqrt{\Big(\frac{l_1-l_0}{2}\Big)^2 + \delta^2} - \Big(\frac{l_1-l_0}{2}\Big)\Big)$$

$$F_1 \;=\; 2f_1 * \delta \Big/ \sqrt{\Big(\frac{l_1-l_0}{2}\Big)^2 + \delta^2}$$

For long SMA-wire:

$$f_2 \;=\; (k_{12}-k_{22})x_{a2} + 2k_{22}\Big(\sqrt{\Big(\frac{l_2-l_0}{2}\Big)^2 + \delta^2} - \Big(\frac{l_2-l_0}{2}\Big)\Big)$$

$$F_2 \;=\; 2f_2 * \delta \Big/ \sqrt{\Big(\frac{l_2-l_0}{2}\Big)^2 + \delta^2}$$

In this part of load history of NiTi-wire SMA damper, the relationship of damping force F and displacement δ of NiTi-wire SMA damper can be expressed by

$$\begin{cases} F \;=\; 2f_1 * \delta \Big/ \sqrt{\Big(\frac{l_1-l_0}{2}\Big)^2 + \delta^2} + 2f_2 * \delta \Big/ \sqrt{\Big(\frac{l_2-l_0}{2}\Big)^2 + \delta^2} \\[3mm] f_1 \;=\; 2k_{31}\Big(\sqrt{\Big(\frac{l_1-l_0}{2}\Big)^2 + \delta^2} - \Big(\frac{l_1-l_0}{2}\Big)\Big) \\[3mm] f_2 \;=\; (k_{12}-k_{22})x_{a2} + 2k_{22}\Big(\sqrt{\Big(\frac{l_2-l_0}{2}\Big)^2 + \delta^2} - \Big(\frac{l_2-l_0}{2}\Big)\Big) \end{cases} \qquad (\delta_3 < \delta \le \delta_4) \qquad (11)$$

e. Unload period of NiTi-wire SMA damper. $\delta_4 \le \delta \le 0$. When deformation of long wire x_2 gets to x_{b2}, unload period of NiTi-wire SMA damper starts.

For short SMA-wire:

$$f_1 \;=\; k_{31}x_1 \;=\; 2k_{31}\Big(\sqrt{\Big(\frac{l_1-l_0}{2}\Big)^2 + \delta^2} - \Big(\frac{l_1-l_0}{2}\Big)\Big)$$

$$F_1 \;=\; 2f_1 * \delta \Big/ \sqrt{\Big(\frac{l_1-l_0}{2}\Big)^2 + \delta^2}$$

For long SMA-wire:

$$f_2 \;=\; k_{32}x_2 \;=\; 2k_{32}\Big(\sqrt{\Big(\frac{l_2-l_0}{2}\Big)^2 + \delta^2} - \Big(\frac{l_2-l_0}{2}\Big)\Big)$$

$$F_2 \;=\; 2f_2 * \delta \Big/ \sqrt{\Big(\frac{l_2-l_0}{2}\Big)^2 + \delta^2}$$

In this part of load history of NiTi-wire SMA damper, the relationship of damping force F and displacement δ of NiTi-wire SMA damper can be expressed by

$$\begin{cases} F = 2f_1 * \delta / \sqrt{\left(\dfrac{l_1 - l_0}{2}\right)^2 + \delta^2} + 2f_2 * \delta / \sqrt{\left(\dfrac{l_2 - l_0}{2}\right)^2 + \delta^2} \\[4mm] f_1 = 2k_{31}\left(\sqrt{\left(\dfrac{l_1 - l_0}{2}\right)^2 + \delta^2} - \left(\dfrac{l_1 - l_0}{2}\right)\right) \qquad (\delta_4 \geq \delta \geq 0) \\[4mm] f_2 = 2k_{32}\left(\sqrt{\left(\dfrac{l_2 - l_0}{2}\right)^2 + \delta^2} - \left(\dfrac{l_2 - l_0}{2}\right)\right) \end{cases} \tag{12}$$

In one load cycle of tension, the relationship between damping force F and displacement δ of NiTi-wire SMA damper can be expressed by Eqs. (3)-(8). When the NiTi-wire SMA damper is compressed, the above Eqs. (3)-(8) can be used to express the relationship between F and δ.

5.1.2 Influence of different NiTi-wire SMA damper parameters on tension-compression energy dissipation ability of NiTi-wire SMA damper

Length of short SMA wire l_1 and length of long SMA wire l_2 can be expressed by d_1, d_2 (Fig. 1) and D (Diameter of steel ring in Fig. 1) in Eq. (13).

$$\begin{cases} l_1 = 2\sqrt{\left(\dfrac{D}{2}\right)^2 - (d_1 + d_2)^2} \\[4mm] l_2 = 2\sqrt{\left(\dfrac{D}{2}\right)^2 - d_2^2} \end{cases} \tag{13}$$

Influence of parameters d_1, d_2 and l_{p0} (Fig. 1) on tension energy dissipation ability of NiTi-wire SMA damper, developed in this paper, will be discussed in this section. Influence of parameters d_1, d_2 and l_{p0} (Fig. 1) on compression energy dissipation ability of NiTi-wire SMA damper is similar to those on tension energy dissipation ability of it, and are therefore not shown here.

When $l_{p0} = 70$ mm, $d_1 = 30$ mm, $d_2 = 30$ mm, the $F{\sim}\delta$ curve (Fig. 15) can be got by Eqs. (3)-(13).
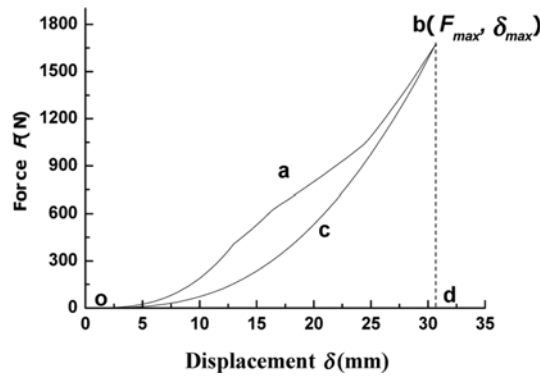

Fig. 15 $F{\sim}\delta$ curve ($l_{p0} = 70$ mm, $d_1 = 30$ mm, $d_2 = 30$ mm)

When d_1, d_2 and l_{p0} were different values, the $F{\sim}\delta$ curves showed similar shapes, and are therefore not shown.

The energy dissipation ratio η of NiTi-wire SMA damper is defined as

$$\eta = \frac{E_d}{E_w} \tag{14}$$

where E_d ('d' means *dissipated* vibration energy) is the area of "*oabco*" in Fig. 15, and E_w ('w' means *whole* vibration energy) is the area of "*oabdo1*" in Fig. 15.

The influences of l_{p0}, d_1 and d_2 on energy dissipation ratio η are shown by Figs. 16-18. The influences of l_{p0}, d_1 and d_2 on the maximum damping force F_{max} (see Fig. 15) and the maximum displacement δ_{max} are shown by Figs. 19-21.

The influence of l_{p0} on η, F_{max} and δ_{max} ($d_1 = 30$ mm, $d_2 = 30$ mm) are illustrated by Table 2. The influence of d_1 on η, F_{max} and δ_{max} ($l_{p0} = 70$ mm, $d_2 = 30$ mm) can be found in Table 3. The influence of d_2 on η, F_{max} and δ_{max} ($l_{p0} = 70$ mm, $d_1 = 30$ mm) are shown by Table 4.

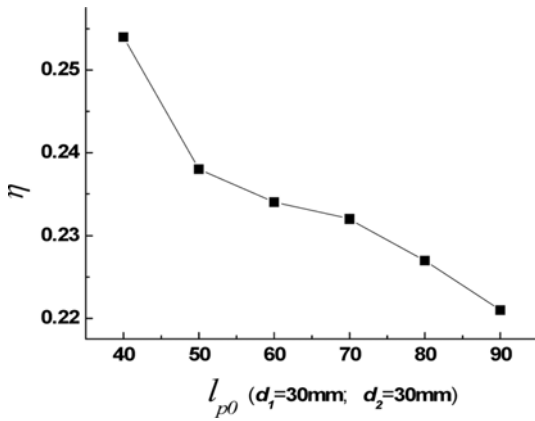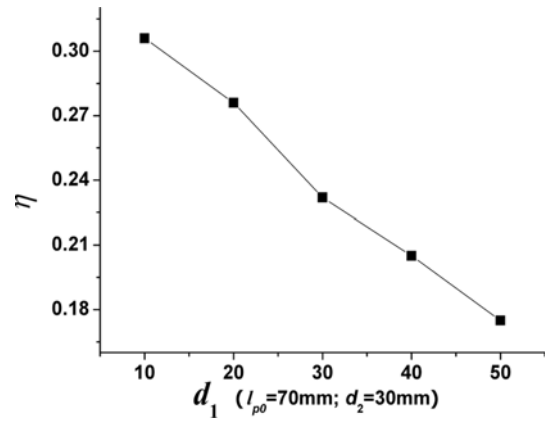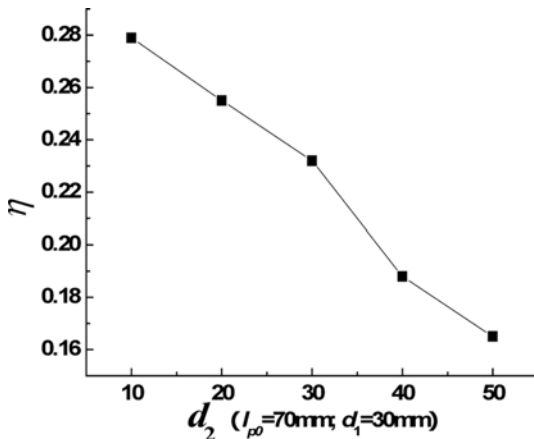Fig. 16 $\eta{\sim}l_{p0}$
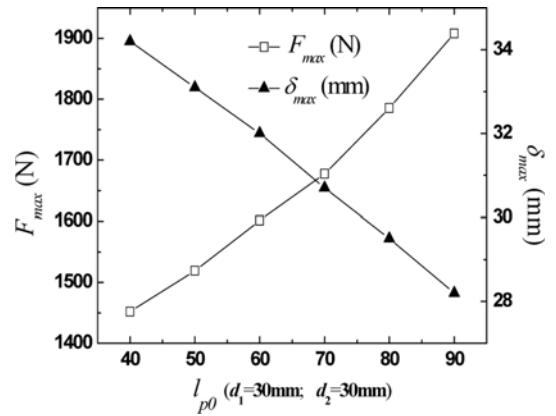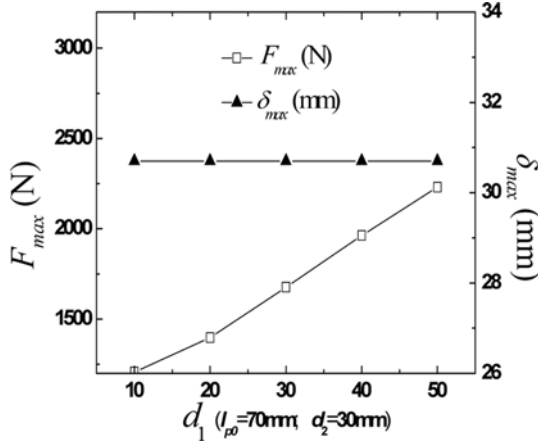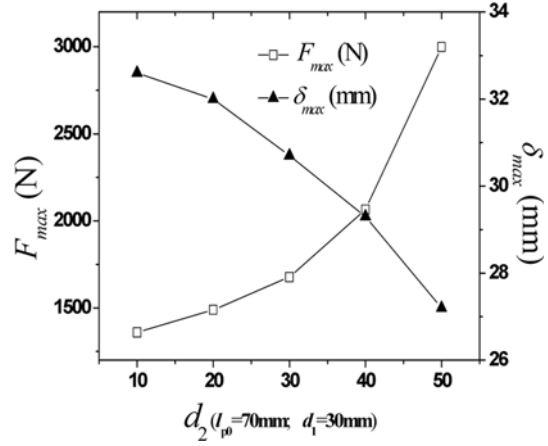

Fig. 17 $\eta{\sim}d_1$

Fig. 18 $\eta{\sim}d_2$

Fig. 19 $F_{max}{\sim}l_{p0}$ and $\delta_{max}{\sim}l_{p0}$

Fig. 20 $F_{max} \sim d_1$ and $\delta_{max} \sim d_1$

Fig. 21 $F_{max} \sim d_2$ and $\delta_{max} \sim d_2$

Table 2 Influence of l_{p0} on η, F_{max} and δ_{max} (d_1 = 30 mm, d_2 = 30 mm)

l_{p0} (mm)	40	50	60	70	80	90
η	0.254	0.238	0.234	0.232	0.227	0.221
F_{max} (N)	1451.7	1519.2	1601.1	1677.5	1785.6	1908.1
δ_{max} (mm)	34.2	33.1	32	30.7	29.5	28.2

Table 3 Influence of d_1 on η, F_{max} and δ_{max} (l_{p0} = 70 mm, d_2 = 30 mm)

d_1	10	20	30	40	50
η	0.306	0.276	0.232	0.205	0.175
F_{max} (N)	1206.7	1397.8	1677.5	1963.2	2230.1
δ_{max} (mm)	30.7	30.7	30.7	30.7	30.7

Table 4 Influence of d_2 on η, F_{max} and δ_{max} (l_{p0} = 70 mm, d_1 = 30 mm)

d_2	10	20	30	40	50
η	0.279	0.255	0.232	0.188	0.165
F_{max} (N)	1359.7	1489.3	1677.5	2065.5	2998.6
δ_{max} (mm)	32.6	32	30.7	29.3	27.2

Based on Figs. 16-18 and Tables 2-4, η decreases when only one of l_{p0}, d_1 and d_2 increases. Based on Figs. 19-21 and Tables 2-4, F_{max} increases when only one of l_{p0}, d_1 and d_2 increases. Based on Figs. 19 and 21, Tables 2 and 4, δ_{max} decreases when only one of l_{p0} and d_2 increases. Based on Fig. 20 and Table 3, δ_{max} is constant, independent of d_1. The reason for this independence is that the above analytical results were based on the same condition that the long SMA wire of the analyzed NiTi-wire SMA dampers is deformed along the same force-deformation path $o \rightarrow a \rightarrow b \rightarrow o$ (Fig. 6). Both η and F_{max} are sensitive to l_{p0}, d_1 and d_2 (Figs. 16-21, Tables 2-4). δ_{max} is sensitive to l_{p0} and d_2 (Figs. 19 and 21, Tables 2 and 4). The analytical results of the eight reduced-scale

dampers were similar to that of the measured results. When the NiTi-wire SMA damper is compressed, the above conclusions can still be used.

5.2 Torsion damping analysis of NiTi-wire SMA damper

5.2.1 Relationship between damping torque T and angle displacement θ of NiTi-wire SMA damper

When a torque applied on the long steel pipe of the developed Niti-wire SMA damper (Fig. 1), the long steel pipe and the steel ring (Fig. 1) will have a relative angle displacement θ.

The relationship between deformation x_i of NiTi-wire and θ can be expressed by Eq. (15).

$$x_i = 2\left[\sqrt{\left(\frac{l_{p0}}{2}\right)^2 + \left(\frac{l_i}{2}\right)^2 - 2 * \frac{l_i}{2} * \frac{l_{p0}}{2} * \cos\theta} - \left(\frac{l_i - l_{p0}}{2}\right)\right] \quad (0 < \theta < \pi, i = 1, 2) \quad (15)$$

where x_1 is deformation of short SMA-wire, x_2 is deformation of long SMA-wire (see Fig. 1).

a. When $x_1 = x_a = 2.3l_1/100$, and $\theta = \theta_1$, then we can get the following equations from Eq. (15).

$$\frac{2.3l_1}{100} = 2\left[\sqrt{\left(\frac{l_{p0}}{2}\right)^2 + \left(\frac{l_1}{2}\right)^2 - 2 * \frac{l_1}{2} * \frac{l_{p0}}{2} * \cos\theta_1} - \left(\frac{l_1 - l_{p0}}{2}\right)\right], \quad \text{then}$$

$$\theta_1 = \arccos\frac{2\left\{\left(\frac{l_{p0}}{2}\right)^2 + \left(\frac{l_1}{2}\right)^2 + \left[\frac{2.3l_1}{200} + \frac{l_1 - l_{p0}}{2}\right]^2\right\}}{l_1 l_{p0}} \quad (16)$$

b. When $x_2 = x_a = 2.3l_2/100$, and $\theta = \theta_2$, then we can get the following equations from Eq. (15).

$$\frac{2.3l_2}{100} = 2\left[\sqrt{\left(\frac{l_{p0}}{2}\right)^2 + \left(\frac{l_2}{2}\right)^2 - 2 * \frac{l_2}{2} * \frac{l_{p0}}{2} * \cos\theta_2} - \left(\frac{l_2 - l_{p0}}{2}\right)\right], \quad \text{then}$$

$$\theta_2 = \arccos\frac{2\left\{\left(\frac{l_{p0}}{2}\right)^2 + \left(\frac{l_2}{2}\right)^2 + \left[\frac{2.3l_2}{200} + \frac{l_2 - l_{p0}}{2}\right]^2\right\}}{l_2 l_{p0}} \quad (17)$$

c. When $x_1 = x_b = 7.8l_1/100$, and $\theta = \theta_3$, then we can get the following equation from Eq. (15).

$$\theta_3 = \arccos\frac{2\left\{\left(\frac{l_{p0}}{2}\right)^2 + \left(\frac{l_1}{2}\right)^2 + \left[\frac{7.8l_1}{200} + \frac{l_1 - l_{p0}}{2}\right]^2\right\}}{l_1 l_{p0}} \quad (18)$$

d. When $x_2 = x_b = 7.8l_2/100$, and $\theta = \theta_4$, then we can get the following equation from Eq. (15).

$$\theta_4 = \arccos\frac{2\left\{\left(\frac{l_{p0}}{2}\right)^2 + \left(\frac{l_2}{2}\right)^2 + \left[\frac{7.8l_2}{200} + \frac{l_2 - l_{p0}}{2}\right]^2\right\}}{l_2 l_{p0}} \quad (19)$$

When the Niti-wire SMA damper is loaded, the load history can be divided into the following parts.

a. For $0 \le \theta \le \theta_1$, the relationship between damping torque T and corresponding angle displacement θ can be expressed by Eq. (20), which was got by similar way illustrated in Section 5.3 of this paper.

$$
\begin{cases}
T = 2f_1 * \dfrac{l_1}{2} * \dfrac{l_{p0}}{2} * \sin\theta / \sqrt{\left(\dfrac{l_1}{2}\right)^2 + \left(\dfrac{l_{p0}}{2}\right)^2 - 2 * \dfrac{l_1}{2} * \dfrac{l_{p0}}{2} * \cos\theta} + \\[2ex]
\qquad 2f_2 * \dfrac{l_2}{2} * \dfrac{l_{p0}}{2} * \sin\theta / \sqrt{\left(\dfrac{l_2}{2}\right)^2 + \left(\dfrac{l_{p0}}{2}\right)^2 - 2 * \dfrac{l_2}{2} * \dfrac{l_{p0}}{2} * \cos\theta} \\[2ex]
f_1 = k_{11} * 2\left[\sqrt{\left(\dfrac{l_{p0}}{2}\right)^2 + \left(\dfrac{l_1}{2}\right)^2 - 2 * \dfrac{l_1}{2} * \dfrac{l_{p0}}{2} * \cos\theta} - \left(\dfrac{l_1 - l_{p0}}{2}\right)\right] \\[2ex]
f_2 = k_{12} * 2\left[\sqrt{\left(\dfrac{l_{p0}}{2}\right)^2 + \left(\dfrac{l_2}{2}\right)^2 - 2 * \dfrac{l_2}{2} * \dfrac{l_{p0}}{2} * \cos\theta} - \left(\dfrac{l_2 - l_{p0}}{2}\right)\right]
\end{cases}
\quad (0 \le \theta \le \theta_1) \quad (20)
$$

b. For $\theta_1 \le \theta \le \theta_2$

$$
\begin{cases}
T = 2f_1 * \dfrac{l_1}{2} * \dfrac{l_{p0}}{2} * \sin\theta / \sqrt{\left(\dfrac{l_1}{2}\right)^2 + \left(\dfrac{l_{p0}}{2}\right)^2 - 2 * \dfrac{l_1}{2} * \dfrac{l_{p0}}{2} * \cos\theta} + \\[2ex]
\qquad 2f_2 * \dfrac{l_2}{2} * \dfrac{l_{p0}}{2} * \sin\theta / \sqrt{\left(\dfrac{l_2}{2}\right)^2 + \left(\dfrac{l_{p0}}{2}\right)^2 - 2 * \dfrac{l_2}{2} * \dfrac{l_{p0}}{2} * \cos\theta} \\[2ex]
f_1 = (k_{11} - k_{21})x_{a1} + k_{21} * 2\left[\sqrt{\left(\dfrac{l_{p0}}{2}\right)^2 + \left(\dfrac{l_1}{2}\right)^2 - 2 * \dfrac{l_1}{2} * \dfrac{l_{p0}}{2} * \cos\theta} - \left(\dfrac{l_1 - l_{p0}}{2}\right)\right] \\[2ex]
f_2 = k_{12} * 2\left[\sqrt{\left(\dfrac{l_{p0}}{2}\right)^2 + \left(\dfrac{l_2}{2}\right)^2 - 2 * \dfrac{l_2}{2} * \dfrac{l_{p0}}{2} * \cos\theta} - \left(\dfrac{l_2 - l_{p0}}{2}\right)\right]
\end{cases}
\quad (\theta_1 \le \theta \le \theta_2) \quad (21)
$$

c. For $\theta_2 \le \theta \le \theta_3$

$$
\begin{cases}
T = 2f_1 * \dfrac{l_1}{2} * \dfrac{l_{p0}}{2} * \sin\theta / \sqrt{\left(\dfrac{l_1}{2}\right)^2 + \left(\dfrac{l_{p0}}{2}\right)^2 - 2 * \dfrac{l_1}{2} * \dfrac{l_{p0}}{2} * \cos\theta} + \\[2ex]
\qquad 2f_2 * \dfrac{l_2}{2} * \dfrac{l_{p0}}{2} * \sin\theta / \sqrt{\left(\dfrac{l_2}{2}\right)^2 + \left(\dfrac{l_{p0}}{2}\right)^2 - 2 * \dfrac{l_2}{2} * \dfrac{l_{p0}}{2} * \cos\theta} \\[2ex]
f_1 = (k_{11} - k_{21})x_{a1} + k_{21} * 2\left[\sqrt{\left(\dfrac{l_{p0}}{2}\right)^2 + \left(\dfrac{l_1}{2}\right)^2 - 2 * \dfrac{l_1}{2} * \dfrac{l_{p0}}{2} * \cos\theta} - \left(\dfrac{l_1 - l_{p0}}{2}\right)\right] \\[2ex]
f_2 = (k_{12} - k_{22})x_{a2} + k_{22} * 2\left[\sqrt{\left(\dfrac{l_{p0}}{2}\right)^2 + \left(\dfrac{l_2}{2}\right)^2 - 2 * \dfrac{l_2}{2} * \dfrac{l_{p0}}{2} * \cos\theta} - \left(\dfrac{l_2 - l_{p0}}{2}\right)\right]
\end{cases}
\quad (\theta_2 \le \theta \le \theta_3) \quad (22)
$$

d. For $\theta_3 \leq \theta \leq \theta_4$

$$
\begin{cases}
T = 2f_1 * \dfrac{l_1}{2} * \dfrac{l_{p0}}{2} * \sin\theta / \sqrt{\left(\dfrac{l_1}{2}\right)^2 + \left(\dfrac{l_{p0}}{2}\right)^2 - 2 * \dfrac{l_1}{2} * \dfrac{l_{p0}}{2} * \cos\theta} + \\[4mm]
\quad 2f_2 * \dfrac{l_2}{2} * \dfrac{l_{p0}}{2} * \sin\theta / \sqrt{\left(\dfrac{l_2}{2}\right)^2 + \left(\dfrac{l_{p0}}{2}\right)^2 - 2 * \dfrac{l_2}{2} * \dfrac{l_{p0}}{2} * \cos\theta} \\[4mm]
f_1 = k_{31} * 2\left[\sqrt{\left(\dfrac{l_{p0}}{2}\right)^2 + \left(\dfrac{l_1}{2}\right)^2 - 2 * \dfrac{l_1}{2} * \dfrac{l_{p0}}{2} * \cos\theta} - \left(\dfrac{l_1 - l_{p0}}{2}\right)\right] \\[4mm]
f_2 = (k_{12} - k_{22})x_{a2} + k_{22} * 2\left[\sqrt{\left(\dfrac{l_{p0}}{2}\right)^2 + \left(\dfrac{l_2}{2}\right)^2 - 2 * \dfrac{l_2}{2} * \dfrac{l_{p0}}{2} * \cos\theta} - \left(\dfrac{l_2 - l_{p0}}{2}\right)\right]
\end{cases}
\quad (\theta_3 \leq \theta \leq \theta_4) \quad (23)
$$

e. Unload period of NiTi-wire SMA damper ($\theta_4 \leq \theta \leq 0$)

$$
\begin{cases}
T = 2f_1 * \dfrac{l_1}{2} * \dfrac{l_{p0}}{2} * \sin\theta / \sqrt{\left(\dfrac{l_1}{2}\right)^2 + \left(\dfrac{l_{p0}}{2}\right)^2 - 2 * \dfrac{l_1}{2} * \dfrac{l_{p0}}{2} * \cos\theta} + \\[4mm]
\quad 2f_2 * \dfrac{l_2}{2} * \dfrac{l_{p0}}{2} * \sin\theta / \sqrt{\left(\dfrac{l_2}{2}\right)^2 + \left(\dfrac{l_{p0}}{2}\right)^2 - 2 * \dfrac{l_2}{2} * \dfrac{l_{p0}}{2} * \cos\theta} \\[4mm]
f_1 = k_{31} * 2\left[\sqrt{\left(\dfrac{l_{p0}}{2}\right)^2 + \left(\dfrac{l_1}{2}\right)^2 - 2 * \dfrac{l_1}{2} * \dfrac{l_{p0}}{2} * \cos\theta} - \left(\dfrac{l_1 - l_{p0}}{2}\right)\right] \\[4mm]
f_2 = k_{32} * 2\left[\sqrt{\left(\dfrac{l_{p0}}{2}\right)^2 + \left(\dfrac{l_2}{2}\right)^2 - 2 * \dfrac{l_2}{2} * \dfrac{l_{p0}}{2} * \cos\theta} - \left(\dfrac{l_2 - l_{p0}}{2}\right)\right]
\end{cases}
\quad (\theta_4 \geq \theta \geq 0) \quad (24)
$$

In one load cycle of torsion of NiTi-wire SMA damper, the relationship between T and θ can be expressed by Eqs. (16)-(24).

5.2.2 Influence of different NiTi-wire SMA damper parameters on torsion energy dissipation ability of NiTi-wire SMA damper

Length of short SMA wire l_1 and length of long SMA wire l_2 can be expressed by d_1, d_2 (Fig. 1) and D (Diameter of steel ring in Fig. 1) in Eq. (13).

Influence of parameters d_1, d_2 and l_{p0} (Fig. 1) on torsion energy dissipation ability of NiTi-wire SMA damper, developed in this paper, will be discussed in this section.

When $l_{p0} = 70$ mm, $d_1 = 30$ mm, $d_2 = 30$ mm, the $T{\sim}\theta$ curve (Fig. 22) can be got by Eqs. (16)-(24). When d_1, d_2 and l_{p0} were different values, the $T{\sim}\theta$ curves showed similar shapes, and are therefore not shown. When $-\pi \leq \theta \leq 0$, the shape of $T{\sim}\theta$ curve is as same as the figure shown in Fig. 22, and are therefore not shown here.

Depending on Eqs. (16)-(24), the influences of l_{p0}, d_1 and d_2 on energy dissipation ratio η are shown by Figs. 23-25; the influences of l_{p0}, d_1 and d_2 on the maximum damping force $T_{\max}$ (see Fig. 22) and the maximum displacement $\theta_{\max}$ are shown by Figs. 26-28.
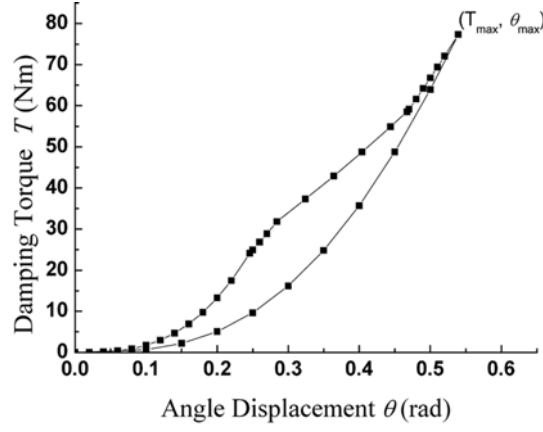
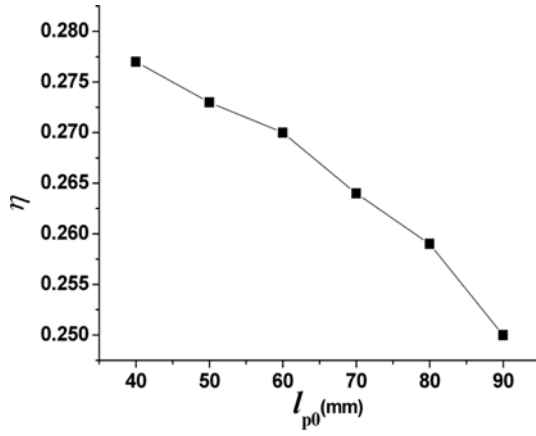Fig. 22 $T \sim \theta$ (l_{p0} = 70 mm, d_1 = 30 mm, d_2 = 30 mm)
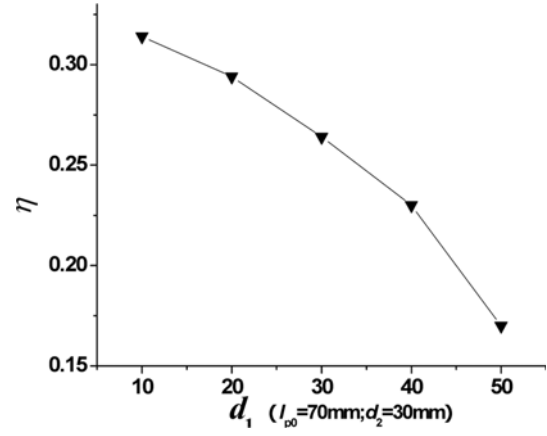

Fig. 23 $\eta \sim l_{p0}$ (Torsion Damping)
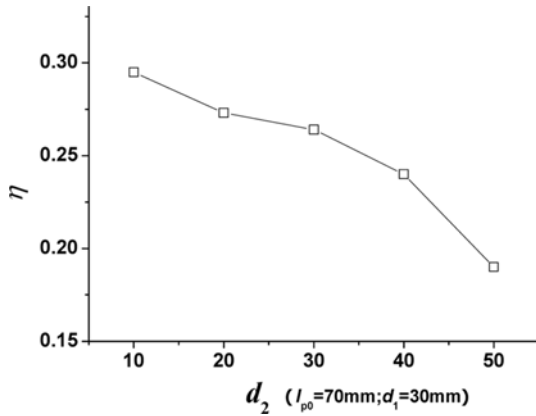

Fig. 24 $\eta \sim d_1$ (Torsion Damping)
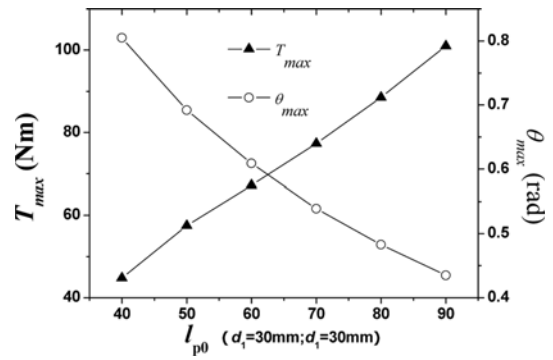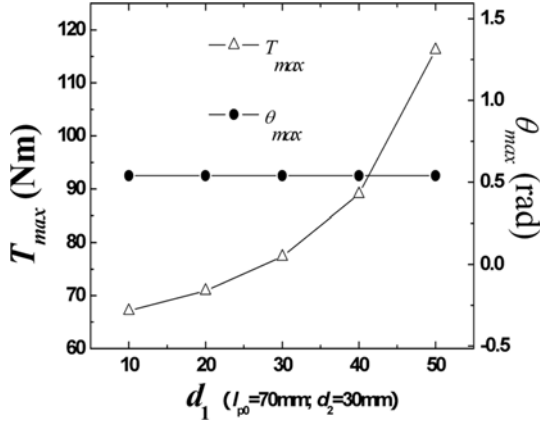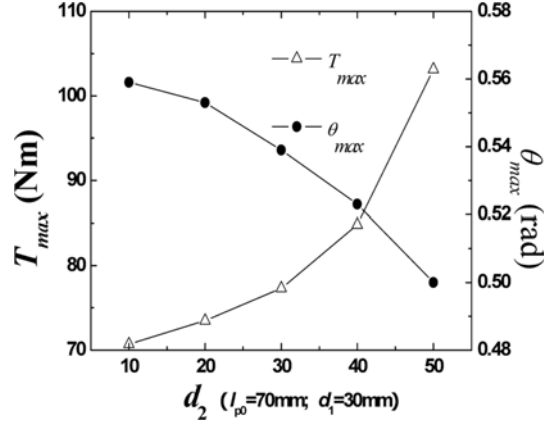

Fig. 25 $\eta \sim d_2$ (Torsion Damping)

Fig. 26 T_{max}, $\theta_{max} \sim l_{p0}$ (Torsion Damping)

Fig. 27 T_{max}, $\theta_{max} \sim d_1$ (Torsion Damping)

Fig. 28 T_{max}, $\theta_{max} \sim d_2$ (Torsion Damping)

The influence of l_{p0} on η, T_{max} and θ_{max} ($d_1 = 30$ mm, $d_2 = 30$ mm) are illustrated by Table 5. The influence of d_1 on η, T_{max} and θ_{max} ($l_{p0} = 70$ mm, $d_2 = 30$ mm) can be found in Table 6. The influence of d_2 on η, T_{max} and θ_{max} ($l_{p0} = 70$ mm, $d_1 = 30$ mm) are shown by Table 7.

Based on Figs. 23-25 and Tables 5-7, η decreases when only one of l_{p0}, d_1 and d_2 increases. Based on Figs. 26-28 and Tables 5-7, T_{max} increases when only one of l_{p0}, d_1 and d_2 increases. Based on Figs. 26 and 28, Tables 5 and 7, θ_{max} increases when only one of l_{p0} and d_2 increases. Based on Fig. 26 and Table 6, θ_{max} is constant, independent of d_1. The reason for this independence is that the above analytical results were based on the same condition that the long SMA wire of the

Table 5 Influence of l_{p0} on η, T_{max} and θ_{max} ($d_1 = 30$ mm, $d_2 = 30$ mm)

l_{p0} (mm)	40	50	60	70	80	90
η	0.277	0.273	0.27	0.264	0.259	0.25
T_{max} (Nm)	44.75	57.51	67.22	77.32	88.51	101.03
θ_{max} (rad)	0.805	0.692	0.609	0.539	0.483	0.435

Table 6 Influence of d_1 on η, T_{max} and θ_{max} ($l_{p0} = 70$ mm, $d_2 = 30$ mm)

d_1	10	20	30	40	50
η	0.314	0.294	0.264	0.23	0.17
T_{max} (Nm)	67.1	70.9	77.32	89.03	116.19
θ_{max} (rad)	0.539	0.539	0.539	0.539	0.539

Table 7 Influence of d_2 on η, T_{max} and θ_{max} ($l_{p0} = 70$ mm, $d_1 = 30$ mm)

d_2	10	20	30	40	50
η	0.295	0.273	0.264	0.24	0.19
T_{max} (Nm)	70.7	73.48	77.32	84.82	103.13
θ_{max} (rad)	0.559	0.553	0.539	0.523	0.5

analyzed NiTi-wire SMA dampers are deformed along the same force-deformation path $o \rightarrow a \rightarrow b \rightarrow o$ (Fig. 6). Both η and T_{max} are sensitive to l_{p0}, d_1 and d_2 (Figs. 16 and 21, Tables 2 and 4). θ_{max} is sensitive to l_{p0} and d_2 (Figs. 19 and 21, Tables 2 and 4). The analytical results of the eight reduced-scale dampers were similar to that of the measured results. When the NiTi-wire SMA damper is turn in the opposite direction, the above conclusions can still be used.

6. Conclusions

In this study, an SMA damper was developed that uses wires made of an SMA alloy, NiTi, to simultaneously damp tension, compression, and torsion. Eight reduced-scale NiTi-wire SMA dampers of different diameter were constructed. Damping force and vibration energy dissipation ability of these dampers in tension, compression, and torsion (i.e., displacement, angle displacement, deformation, restoring force, damping force, and damping torque) were measured, and then compared with analytical results based on a model of pseudoelasticity restoring force for an SMA wire and on tension, compression, and torsion analysis.

The characteristics of the eight reduced-scale dampers (energy dissipation ratio, damping force, damping torque, displacement, and angle displacement) were measured. The measured data revealed that all of the eight reduced-scale dampers could damp tension, compression, and torsion and indicates that the developed NiTi-wire SMA damper could simultaneously damp tension, compression, and torsion.

The analytical results revealed the following features of the NiTi-wire SMA dampers. The energy dissipation ratio η for the dampers decreases when only one of parameters (l_{p0}, d_1 and d_2) of SMA damper increases. When distance d_1 between two SMA wires of SMA damper increased, both the maximum damping force F_{max} and the maximum damping torque T_{max} increased sensitively. The maximum displacement δ_{max} and the maximum angle displacement θ_{max} almost were independent of d_1. The reason for this independence is that the measured and analytical results of all dampers were based on the same condition that the long SMA wire of all the measured NiTi-wire SMA dampers was deformed along the same force-deformation path. The energy dissipation ratio η for the dampers decreases when d_1 increases.

Both the analytical results and measured results verify the tension, compression, and torsion damping ability of the NiTi-wire SMA damper developed here.

Acknowledgements

References

Adachi, Y., Unjoh, S. and Kondoh, M. (2000), "Development of a shape memory alloy damper for intelligent bridge systems", *Shape Memory Materials Science Forum*, **327**(3), 31-34.
Aiken, I.D., Nims, D.K., Whittaker, A.S. and Kelly, J.M. (1993), "Testing of passive energy dissipation systems",

Earthquake Spectra, **9**, 335-369.

Dolce, M., Cardone, D. and Marnetto, R. (2000), "Implementation and testing of passive control devices based on shape memory alloys", *Earthq. Eng. Struct. Dyn.*, **29**, 945-968.

Duval, L., Noori, M.N., Hou, Z., Davoodi, H. and Seelecke, S. (2000), "Random vibration studies of an SDOF system with shape memory restoring force", *PHYSICA B*, **275**(1-3), 138-141.

Graesser, E.J. and Cozzarelli, F.A. (1991), "Shape memory alloys as new material for aseismic isolation", *J. Eng. Mech.*, ASCE, **117**(11), 2590-2608.

Han, Y.-L., Li, A.-Q. and Lin, P.-H. *et al.* (2000), "Experimental study of frame structure vibration control by using shape memory alloy damper", *J. of Southeast University (Natural Science Edition)* **30**(4), 16-20 (in Chinese).

Han, Y.-L., Li, Q.-S. and Li, A.-Q. *et al.* (2003), "Structural vibration control by shape memory alloy damper", *Earthq. Eng. Struct. Dyn.*, **32**, 483-494.

Hodgson, D.E. and Krumme, R.C. (1994), "Damping in structural application", *Proc. of 1st Int. Conf. on Shape Memory and Superelastic Technologies*, Pacific Grove, CA, USA.

Ip, K.H. (2000), "Energy dissipation in shape memory alloy wires under cyclic bending", *Smart Materials & Structures*, **9**(5), 653-659.

Ostachowicz, W.M. and Kaczmarczyk, S. (2001) "Vibrations of composite plates with SMA fibres in a gas stream with defects of the type of delamination", *Comp. Struct.*, **54**(2-3), 305-311.

Saadat, S., Noori, M. and Davoodi, H. *et al.* (2001), "Using NiTi SMA tendons for vibration control of coastal structures", *Smart Materials and Structures*, **10**(4), 695-704.

Tamai, H. and Kitagawa, Y. (2002), "Pseudoelastic behavior of shape memory alloy wire and its application to seismic resistance member for building", *Computational Materials Science*, **25**(1-2), 218-227.

Torra, V., Isalgue, A., Lovey, F.C. and Sade, M. (2002), "Damping via Cu-Zn-Al shape memory alloys (SMA): The action of diffusive effects on the macroscopic description", *Proc. of SPIE - The Int. Society for Optical Engineering* v4696 Mar 18-20. Sponsored by: SPIE The International Society for Optical Engineering, 186-196.

Van Humbeeck, J. and Liu, Y. (2000), "Shape memory alloys as damping materials", *Shape Memory Materials Science Forum*, **327**(3), 331-338.

Williams, K.A., Chiu, G.T.-C. and Bernhard, R.J. (2005), "Dynamic modeling of a shape memory alloy adaptive tuned vibration absorber", *J. Sound Vib.*, **280**(1-2), 211-234.

Witting, P.R. and Cozzarelli, F.A. (1992), "Shape memory structural dampers: material properties, design and seismic testing", NCEER Report, No.92/13, State University of New York, Buffalo, USA.